The Morphology and Dynamics of the Viscoelastic Microphase Separation of Diblock Copolymers

Yanli Huo,† Hongdong Zhang,† and Yuliang Yang*,†,‡

Department of Macromolecular Science, Key Lab of Molecular Engineering of Polymers, Ministry of Education of China, and Department of Physics, Fudan University, Shanghai 200433, China

Received September 18, 2002; Revised Manuscript Received April 21, 2003

ABSTRACT: In this paper, the kinetics and morphology of viscoelastic microphase separation of diblock copolymers are investigated in detail. It is found that for a symmetric system ($f = 0.5$), taking into account the bulk modulus differences between the two blocks, the classical randomly oriented lamellar morphology is not observed. Instead, we find that droplets of the lower bulk modulus soft block disperse in a matrix of higher bulk modulus hard block. In the case of off-critical system ($f = 0.4$), since an inherent composition asymmetry exists between the two blocks, the viscoelastic microphase separated morphology is also different from that normally observed, whether there is an apparent difference in the bulk moduli between two blocks. However, when a bulk modulus difference exists between the two blocks, the morphology is further altered. Addition of random thermal noise to both the critical ($f = 0.5$) and the off-critical system ($f = 0.4$) weakens the suppression of concentration fluctuations, but no fundamental structural transformation is caused by the noise. Since the abnormal morphology is observed on slow approach to the equilibrium state, we conclude that the viscoelastic effect may be largely responsible for the observed deviations between the experimentally measured and the mean-field theoretically calculated phase diagrams.

I. Introduction

Viscoelasticity is an intrinsic property of polymers, and the effects of polymer viscoelasticity on the kinetics and morphology of phase separation of polymer blends have been intensively studied over the past 2 decades. The effects of viscoelasticity on the early stage of phase separation were first noticed by DeGennes et al.[1−4] in an investigation of concentration fluctuation dynamics of polymer solutions. Binder et al.[5] investigated the early stages of viscoelastic phase separation in a binary mixture by coupling a slow relaxation variable to the linearized Cahn−Hilliard theory. At that time, it was believed that viscoelasticity affects only the early stages of phase separation, since, at this stage, the phase separation kinetics is slower than the rates of chain disentanglement.[6−8] To examine the effects of viscoelasticity during the middle and late stages of phase separation, Doi and Onuki[9,10] proposed a two-fluid model to describe the dynamic coupling between stress and composition fluctuation in polymer mixtures. Up to now, the two-fluid model has been successfully applied to the analysis of the effects of viscoelasticity in the early stages of spinodal decomposition of polymer mixtures by Onuki and Taniguchi[11] and Kumaran and Frederickson.[12]

The effects of viscoelasticity on the late stages of phase separation were ignored until Tanaka[13−15] observed some unusual experimental patterns in the phase separation of polymer solutions and blends. The appearance of a moving droplet phase and networklike or spongelike patterns in the phase-separating polymer solution and phase inversion in polymer blends where one of the components is close to its glass transition[16] reveal that a dynamical asymmetry between two components could lead to the unusual phase separation behavior. This phenomenon was termed "viscoelastic phase separation" by Tanaka.[17,18]

Along with the experimental observation of unusual morphologies and dynamics of viscoelastic phase separation, computer simulations of phase separating mixtures with strong dynamic asymmetry have also been carried out in order to understand the mechanism of the viscoelastic phase separation. On the basis of different models and algorithms, extensive computer simulations have been done to explain the phenomena experimentally observed.[19−29] For example, Sappelt and Jackle[19−21] simulated the phase separation using the nonlinear Cahn−Hilliard equation with a strongly concentration-dependent mobility. Taniguchi and Onuki[26] investigated a viscoelastic phase separation based on the two-fluid model by introducing a conformation tensor to represent chain coil deformations during phase separation. Tanaka and Araki's simulation work[27,28] best reproduced essentially all of the features of experimentally observed viscoelastic phase separation. On the basis of the viscoelastic model developed by Tanaka, Zhang et al.[29] investigated in detail the effects of differences in viscoelasticity between two components on the viscoelastic phase separation of polymer solutions.

Although the microphase separation of diblock copolymers has been studied for more than 2 decades,[30−36] viscoelastic effects on the morphology and the dynamics of microphase separation has received little attention and many aspects of viscoelasticity effects on the microphase separation morphology and dynamics remain unclear. For example, although the theoretically calculated phase diagram based on the mean-field theory reproduces the overall topology of the experimentally measured phase diagram, many details of the theoretical phase diagram disagree with experimental

* To whom correspondence should be addressed. E-mail: ylyang@srcap.stc.sh.cn.
† Department of Macromolecular Science, Fudan University.
‡ Department of Physics, Fudan University.

10.1021/ma021504f CCC: $25.00
Published on Web 06/20/2003

results.[37] Concerning the morphology and dynamics of viscoelastic microphase separation, Luo et al.[38] have studied polymer chain stretching effects on the morphology and rheology of microphase separating diblock copolymers under steady shear. In their study, they introduce a free energy function for the chain deformation induced by flow field. However, the viscoelastic microphase separation of diblock copolymers has not been investigated using a more advanced model until the present study.

Our objective in this study is to examine the viscoelastic effects on the morphology and dynamics of microphase separation of diblock copolymers by means of a computer simulation based on the viscoelastic model developed by Tanaka.[17] The simulation results show that both the morphology and dynamics of the microphase separation of diblock copolymers are altered by the viscoelasticity. Therefore, it is plausible that the viscoelastic differences between the two blocks change the details of the phase diagram of diblock copolymers. The results obtained in this study will help us understand the origin of some of the discrepancies between calculated and measured diblock copolymer phase diagrams.

II. Model Equations and Simulation Algorithm

The viscoelastic model adopted here is that developed by Tanaka.[9,17] For a two-component system of A and B, the basic model equations are written as

$$\frac{\partial \phi}{\partial t} = -\nabla\cdot(\phi \mathbf{v}) - \nabla\cdot[\phi(1-\phi)(\mathbf{v}_A - \mathbf{v}_B)] + \epsilon\xi(\mathbf{r},t)$$

$$\mathbf{v}_A - \mathbf{v}_B = -\frac{1-\phi}{\zeta}\left[\phi\nabla\frac{\delta F(\phi)}{\delta\phi} - \nabla\cdot\boldsymbol{\sigma}^{(A)} + \frac{\phi}{1-\phi}\nabla\cdot\boldsymbol{\sigma}^{(B)}\right] \quad (1)$$

$$\rho\frac{\partial \mathbf{v}}{\partial t} \cong -\phi\nabla\frac{\delta F(\phi)}{\delta\phi} + \nabla P + \nabla\cdot\boldsymbol{\sigma}^{(A)} + \nabla\cdot\boldsymbol{\sigma}^{(B)}$$

where ζ is the friction coefficient, being on the order of $6\pi\eta b^{-2}\phi^2$ with b the segment size and η the microscopic viscosity of the system. ϕ is the volume fraction of one component of the polymer mixture, σ is the stress acting on the polymer chain, where the superscripts denote the components A and B, respectively, P is the pressure, $F(\phi)$ is the free energy function, and $\mathbf{v}_A$ and $\mathbf{v}_B$ are the velocities of two components, respectively. The average velocity $\mathbf{v}$ is defined as $\mathrm{v} = \phi_A\mathbf{v}_A + \phi_B\mathbf{v}_B$, with ϕ_A and ϕ_B, respectively, denoting the volume fractions of the two components. The noise term is represented by $\epsilon\xi(\mathbf{r},t)$, where ϵ is the amplitude of the noise. In this work, an order parameter $\psi = \phi_A - \phi_B$ is introduced, and the viscoelastic model can be rewritten as

$$\frac{\partial \psi}{\partial t} = -\nabla\cdot(\psi\mathbf{v}) - \nabla\cdot\left[\frac{1-\psi^2}{2}(\mathbf{v}_A - \mathbf{v}_B)\right] + \epsilon\xi(\mathbf{r},t)$$

$$\mathbf{v}_A - \mathbf{v}_B =$$

$$-\frac{1}{\zeta}\left[\frac{1-\psi^2}{2}\nabla\frac{\delta F(\psi)}{\delta\psi} - \frac{1-\psi}{2}\nabla\cdot\boldsymbol{\sigma}^{(A)} + \frac{1+\psi}{2}\nabla\cdot\boldsymbol{\sigma}^{(B)}\right] \quad (2)$$

$$\rho\frac{\partial \mathbf{v}}{\partial t} \cong -\psi\nabla\frac{\delta F(\psi)}{\delta\psi} + \nabla P + \nabla\cdot\boldsymbol{\sigma}^{(A)} + \nabla\cdot\boldsymbol{\sigma}^{(B)}$$

Although eq 2 is originally derived for a binary polymer mixture, it is not difficult to prove that for diblock copolymers, at the phenomenological level of a two-fluid model, the thermodynamic force (osmotic pressure) in the above equation should be replaced by the free energy of diblock copolymers. It is well-known that the free energy function of diblock copolymers, $F(\psi)$, is given by[39]

$$\begin{aligned} F(\psi) &= F(\psi)_S + F(\psi)_L \\ &= \int d\mathbf{r}\left[-\frac{\tau}{2}\psi^2 + \frac{g}{4}\psi^4 + \frac{K}{2}(\nabla\psi)^2\right] \\ &\quad + \frac{\alpha}{2}\int d\mathbf{r}\int d\mathbf{r}'\, G(\mathbf{r}-\mathbf{r}')[\psi(r)-\bar{\psi}][\psi(\mathbf{r}')-\bar{\psi}] \end{aligned} \quad (3)$$

where G is Green's function that satisfies $\nabla^2 G(\mathbf{r},\mathbf{r}') = -\delta(\mathbf{r}-\mathbf{r}')$. The positive constants τ, g, K, and α are phenomenological parameters. In the above equation, $\bar{\psi}$ is the spatially averaged order parameter. The Laplace transform of the variational derivative of $F(\psi)$ can be written as follows:

$$\begin{aligned} \nabla^2\frac{\delta F(\psi)}{\delta\psi} &= \nabla^2\left(\frac{\delta F(\psi)_S}{\delta\psi} + \frac{\delta F(\psi)_L}{\delta\psi}\right) \\ &= \nabla^2(-\psi + \psi^3 - \nabla^2\psi) - \alpha(\psi - \bar{\psi}) \end{aligned} \quad (4)$$

For the sake of numerical stability and simplicity, the polynomial form of $-\psi + \psi^3 - \nabla^2\psi$ is replaced by $-A\tanh\psi + \psi - D\nabla^2\psi$, which was first used in the cell dynamics scheme (CDS) proposed by Oono and Puri.[40] In the above simplified function, $A \geq 1.0$ is a phenomenological parameter characterizing the quenching depth, D, related to the interfacial free energy, and α is a parameter related to $f = N_A/N$ with $N = N_A + N_B$ being the total chain length of the diblock copolymers. In the present simulation, we set $A = 1.3$, $D = 0.25$, and $\alpha = 0.01$.

The evolution equation for the order parameter can be solved in real space due to the existence of eq 4. However, the evolution equation for the velocity field cannot be solved in real space due to the existence of the term of $\nabla\mu$, where $\mu = \delta F(\psi)/\delta\psi = \delta F(\psi)_S/\delta\psi + \delta F(\psi)_L/\delta\psi = \mu_S + \mu_L$. It is obvious that $\nabla\mu_S$ is easy to calculate since the analytical expression for $\mu_S = -A\tanh\psi + \psi - D\nabla^2\psi$ is already known. However, solving for the $\nabla\mu_L$ field is difficult as only $\nabla^2\mu_L = -\alpha(\psi - \bar{\psi})$ is known. To overcome this difficulty, $\nabla^2\mu_L = -\alpha(\psi - \bar{\psi})$ is rewritten in Fourier space, i.e.,

$$-\mathbf{k}^2\mu_L(\vec{k}) = [-\alpha(\psi - \bar{\psi})]_k \text{ or } \mu_L(\vec{k}) = \frac{[\alpha(\psi - \bar{\psi})]_k}{\mathbf{k}^2} \quad (5)$$

where $\mu_L(\vec{k})$ and $[\alpha(\psi - \bar{\psi})]_k$ are the Fourier transforms of $\mu_L(\mathbf{r})$ and $\alpha(\psi - \bar{\psi})$, respectively. Then, $\mu_L(\mathbf{r})$ can be obtained by the inverse Fourier transform of $\mu_L(\vec{k})$. Therefore, the Navier−Stokes equation in eq 2 can be solved in Fourier space by introducing the transverse operator[41]

$$\rho\frac{\partial \mathbf{v}}{\partial t} = \mathbf{T}_\perp\cdot\left\{-\psi\nabla\frac{\delta F(\psi)}{\delta\psi} + \nabla\cdot\boldsymbol{\sigma}^{(A)} + \nabla\cdot\boldsymbol{\sigma}^{(B)}\right\} \quad (6)$$

where $\mathbf{T}_\perp$ is the transverse operator, and takes a simple form in Fourier space.

$$\mathbf{T}_\perp(\vec{k}) = \mathbf{I} - \frac{\mathbf{k}\mathbf{k}}{\mathbf{k}^2} \quad (7)$$

Here, $\mathbf{T}_{\perp}(\vec{k})$ is the Fourier transform of transverse operator, and $\mathbf{I}$ is the unit tensor.

The stress tensor σ is defined as[17,29]

$$\sigma_{ij}^{(\beta)} = \int_{-\infty}^{t} \mathrm{d}t' \left[G_{\beta s}(t-t') \left(\frac{\partial v_\beta^{\,j}}{\partial x_i} + \frac{\partial v_\beta^{\,i}}{x_j} - \frac{2}{d}(\nabla \cdot \mathbf{v}_\beta)\delta_{ij}^{(\beta)} \right) + G_{\beta b}(t-t')\nabla \cdot \mathbf{v}_\beta(t')\delta_{ij}^{(\beta)} \right] \quad (\beta = \mathrm{A, B}) \quad (8)$$

where d is the spatial dimensionality, and $G_{\beta s}$ and $G_{\beta b}$, respectively, are the shear and bulk relaxation moduli, which are assumed to be Maxwellian with a single relaxation time, as follows:

$$G_{\beta s}(t) = M_{\beta s} \exp(-t/\tau_{\beta s}), \quad G_{\beta b}(t) = M_{\beta b} \exp(-t/\tau_{\beta b}) \quad (\beta = \mathrm{A, B}) \quad (9)$$

In our simulations, the parameters of $M_{\beta s}$, $M_{\beta b}$, $\tau_{\beta s}$, and $\tau_{\beta b}$ are function of ϕ_β (β = A, B),[17,27,29] i.e.,

$$M_{\beta s} = M_{\beta s}{}^0 \phi_\beta{}^2, \quad M_{\beta b} = M_{\beta b}{}^0 \theta(\phi_\beta - \phi_\beta{}^0), \quad \tau_{\beta s} = \tau_{\beta s}{}^0 \phi_\beta{}^2, \quad \tau_{\beta b} = \tau_{\beta b}{}^0 \phi_\beta{}^2 \quad (10)$$

where $\phi_\beta{}^0$ (β = A, B) is the average composition of blocks A and B, respectively. $\theta(\phi_\beta - \phi_\beta{}^0)$ is a step function, which equals 1.0 when ϕ_β is larger than $\phi_\beta{}^0$ and equals zero if ϕ_β is smaller than $\phi_\beta{}^0$. In the simulation, the relaxation times are arbitrarily chosen as $\tau_{\beta s}{}^0 = 10$, $\tau_{\beta b}{}^0 = 50$, and different shear and bulk relaxation moduli are achieved by adjusting the relative magnitudes of the parameters $M_{\beta s}{}^0$ and $M_{\beta b}{}^0$. Thus, instead of solving eq 8, the stresses can be obtained by solving the following equations:[17,27,29]

$$\frac{\partial \boldsymbol{\sigma}_{\beta s}}{\partial t} + \mathbf{v}_\alpha \cdot \nabla \boldsymbol{\sigma}_{\beta s} = \boldsymbol{\sigma}_{\beta s} \cdot \nabla \mathbf{v}_\beta + (\nabla \mathbf{v}_\beta)^T \cdot \boldsymbol{\sigma}_{\beta s} - \frac{1}{\tau_{\beta s}(\phi_\beta)} \sigma_{\beta s} + M_{\beta s}(\phi_\beta)[\nabla \mathbf{v}_\beta + (\nabla \mathbf{v}_\beta)^T] \quad (11)$$

$$\frac{\partial \boldsymbol{\sigma}_{\beta b}}{\partial t} + \mathbf{v}_\beta \cdot \nabla \boldsymbol{\sigma}_{\beta b} = -\frac{1}{\tau_{\beta b}(\phi_\beta)} \sigma_{\beta b} + M_{\beta b}(\phi_\beta) \nabla \cdot \mathbf{v}_\beta \quad (\beta = \mathrm{A, B})$$

The numerical simulations are performed using the Euler scheme in a two-dimensional 128 × 128 square lattice with conserved order parameter and periodic boundary conditions in both directions. The time step is 0.02 to ensure numerical stability, and a random fluctuation in the volume fraction of each lattice site at the start of a simulation is within ±0.001. The additional noise term, which is discussed in section IIIC, below, is neglected in the other cases.

III. Results and Discussions

A. Case of $f = 0.5$. Figure 1 shows the morphological evolution of the viscoelastic microphase separation of a symmetric (f = 0.5) A-*b*-B diblock copolymer with various values of $M_{\beta s}{}^0$ and $M_{\beta b}{}^0$ (β = A or B). For comparison, we also show the pattern evolution of the diblock copolymer without taking viscoelastic effects into account (Figure 1a). The simulation was performed based on the solid model shown as eq 12, which is reduced from eq 2 by assuming $M_{\beta s}{}^0 = M_{\beta b}{}^0 = 0$ and $\mathbf{v} = 0$, as already discussed by Tanaka[17]

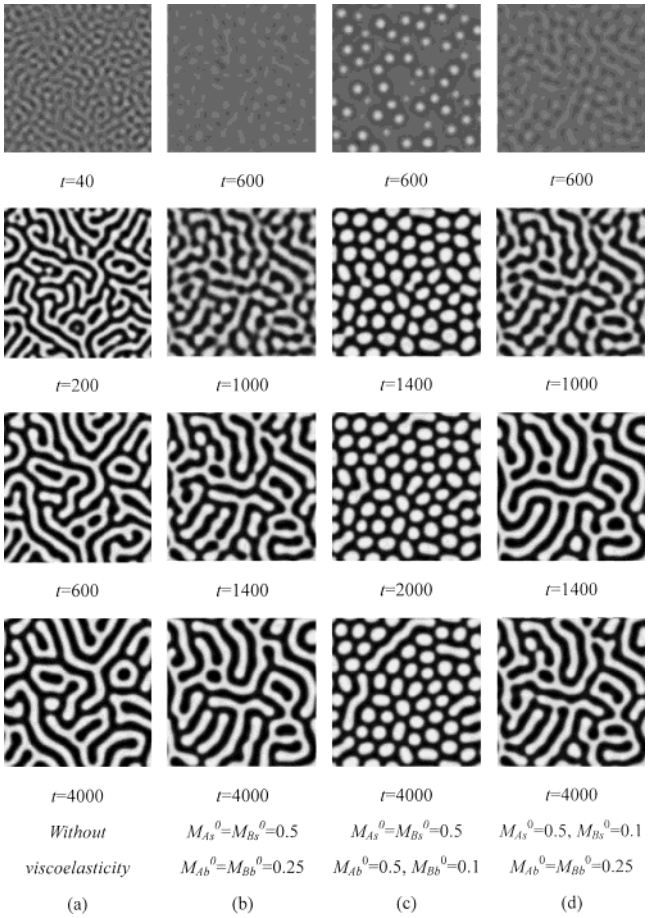

Figure 1. Simulated pattern evolution during microphase separation of diblock copolymers with and without viscoelasticity under critical quench (f = 0.5). A-rich regions are shown by black whereas B-rich regions are shown by white.

$$\frac{\partial \psi}{\partial t} = \frac{1}{4\zeta} \nabla \left[(1-\psi^2)^2 \nabla \frac{\delta F(\psi)}{\delta \psi} \right] \quad (12)$$

It is clear that eq 12 yields a lamellar morphology of random orientation with f = 0.5 (Figure 1a). When $M_{As}{}^0 = M_{Bs}{}^0 = 0.5$, and $M_{Ab}{}^0 = M_{Bb}{}^0 = 0.25$, i.e., where there is no modulus difference between the two blocks, the morphological evolution is slowed due to viscoelastic effects, but a randomly oriented lamellar morphology similar to that of Figure 1a is also obtained (Figure 1b). Figure 1c shows the morphological evolution with the same $M_{\beta s}{}^0$ (β = A and B), but different $M_{Ab}{}^0$ and $M_{Bb}{}^0$, namely, there is a difference between the bulk moduli of the two blocks. It can be seen that the resulting morphology is quite different from those shown in Figure 1, parts a and b. Even though the volume fractions of A and B are identical, i.e., f = 0.5, instead of forming the lamellar morphology, the lower bulk modulus B-rich phase disperses as isolated droplets in the matrix of the higher bulk modulus A-rich phase. It should be noted that the dispersed droplet morphology can be sustained for extremely long times (the morphology of Figure 1c remains almost unchanged even at t = 20 000, as shown in Figure 2). After having investigated the effect of differences in bulk modulus, we focused our attention on differences in shear modulus. It is seen from the results shown in Figure 1d that shear modulus

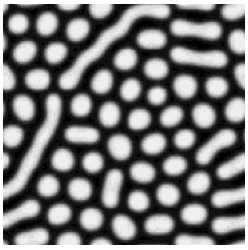

Figure 2. Morphology of Figure 1c after evolved for t = 20 000.

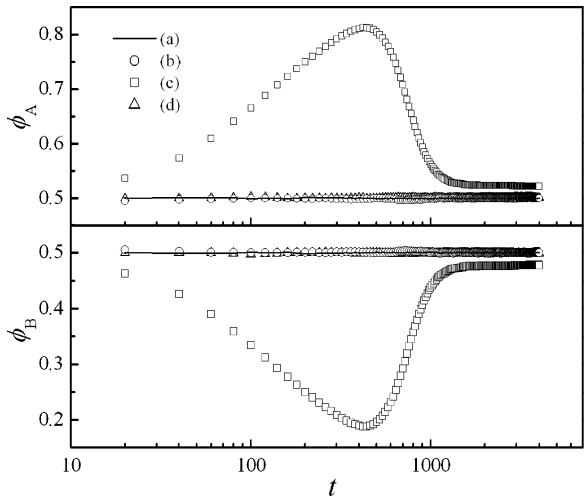

Figure 3. Time evolution in the area fraction ϕ_A of A-rich phase and ϕ_B of B-rich phase. Parts a−d correspond to the cases of Figure 1a−d, respectively.

differences do not lead to a significantly different morphology from that shown in Figure 1b. Therefore, it seems that only differences in bulk modulus play a key role in driving the system away from a normal diblock phase separation. This result agrees with that observed by Tanaka et al.[27] and Zhang et al.[28] in their simulations of polymer solution phase separation.

To investigate the morphology evolution more quantitatively, the temporal change of the area fraction of two phases (ϕ_A and ϕ_B) for the normal microphase separation of diblock copolymers without viscoelasticity and the viscoelastic microphase separation with various values of $M_{\beta s}^0$ and $M_{\beta b}^0$ were investigated, and are shown in Figure 3. One important result of Figure 3 is that when the bulk moduli $M_{\beta b}^0$ (β = A and B) of these two blocks are identical, regardless of whether the shear moduli $M_{\beta s}^0$ of two blocks are identical, the area fractions of both phases always remain at 0.5 during the evolution of the entire microphase separation process, as is true in the case of normal microphase separation of diblock copolymers excluding viscoelastic effects. Correspondingly, for these cases, the morphology is a randomly oriented lamellar pattern. In contrast, for a system with bulk modulus differences between the two blocks, the area fractions of both phases do not remain constant during the morphology evolution, as shown in Figure 3c. As the phase separation proceeds, the area fraction of higher bulk modulus A-rich phase reaches a maximum. Correspondingly, the area fraction of lower bulk modulus B-rich phase reaches a minimum. After the extrema, the area fractions of both phases approach their own steady state values, which are slightly higher than f = 0.5 for the A-rich phase and slightly lower than f = 0.5 for the B-rich phase. Correspondingly, from the pattern evolution shown in Figure 1c, we can see the

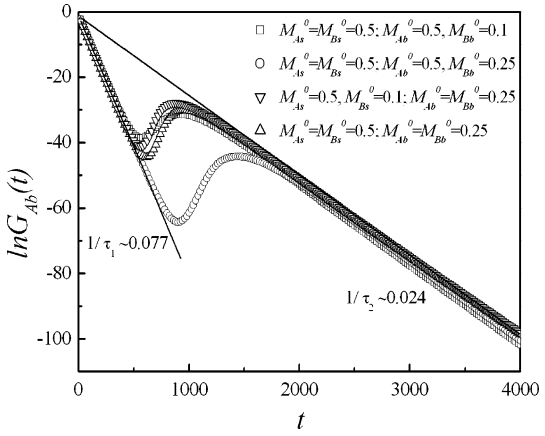

Figure 4. Relaxation of the bulk modulus in the A-rich phase with various values of $M_{\beta s}^0$ and $M_{\beta b}^0$ for the case of f = 0.5.

emergence of the B-rich droplets with lower bulk modulus from the homogeneous state. As time proceeds, the area fraction of the B-rich droplets increases. Even with evolution times as long as t = 20 000 (Figure 2), the B-rich phase maintains its dispersed droplet morphology and the A-rich phase retains its continuous structure. It is surprising that the normal randomly oriented lamellar morphology is still not observed even at f = 0.5 and t = 20 000. It is noteworthy that, in our present study on the f = 0.5 system, the larger the modulus differences between the two blocks, the greater the number of isolated droplets that can be seen. It is clear that this type of abnormal dispersed droplet morphology is metastable; i.e., it will relax to an equilibrium lamellar morphology. However, it appears that it reaches this equilibrium state very slowly. Therefore, for systems with a large bulk modulus differences between the two blocks, the apparent phase diagram could deviate significantly from the phase diagram predicted by the mean field theoretical calculations. It is possible that the viscoelastic effects may be the dominant factor responsible for the discrepancy between the experimentally measured and mean field theoretically calculated phase diagrams.

The temporal relaxation patterns of the bulk modulus of the A-rich phase with various values of $M_{\beta s}^0$ and $M_{\beta b}^0$ are shown in Figure 4. Analogous to the case of polymer solutions,[29] the relaxation process can be divided into three regimes, including two linear regimes and one transition regime. The two linear regimes, which reveal that the modulus relaxation proceeds according to a Maxwell type model, exhibit different relaxation times. During the first linear regime, the inverse relaxation time is on, the order of $1/\tau \sim 0.077$, irrespective of the values of $M_{\beta s}^0$ and $M_{\beta b}^0$. However, the inverse relaxation time for the second linear regime is much longer, on the order of $1/\tau \sim 0.024$. By comparing Figure 4 and Figure 1, it can be seen that the first linear regime corresponds to the early stage in microphase separation, during which concentration fluctuations are strongly suppressed and the B-rich droplet phase is about to emerge from the homogeneous state. However, during the second linear regime, which corresponds to the late stage of phase separation, the concentration fluctuations of the two phases are approaching to their steady state values. The transition between the two linear regimes corresponds to the intermediate stage of phase separation, during which the suppression of the concentration fluctuation is gradually relieved and concentration

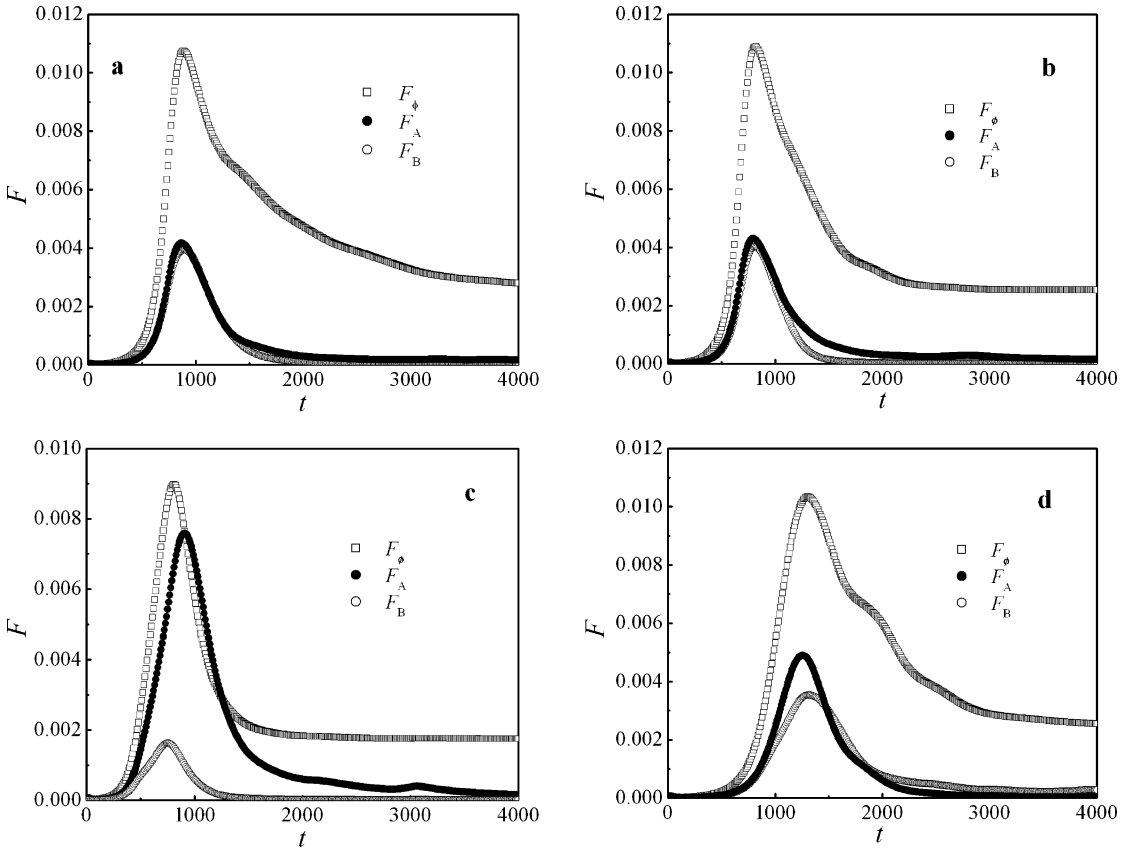

Figure 5. Time evolution in the average magnitudes of the three types of forces with various values of $M_{\beta s}{}^0$ and $M_{\beta b}{}^0$ for the case of $f = 0.5$: (a) $M_{As}{}^0 = M_{Bs}{}^0 = 0.5$, $M_{Ab}{}^0 = M_{Bb}{}^0 = 0.25$; (b) $M_{As}{}^0 = 0.5$, $M_{Bs}{}^0 = 0.1$, $M_{Ab}{}^0 = M_{Bb}{}^0 = 0.25$; (c) $M_{As}{}^0 = M_{Bs}{}^0 = 0.5$, $M_{Ab}{}^0 = 0.5$, $M_{Bb}{}^0 = 0.1$; (d) $M_{As}{}^0 = M_{Bs}{}^0 = 0.5$, $M_{Ab}{}^0 = 0.5$, $M_{Bb}{}^0 = 0.25$.

fluctuations rapidly increase. It should be pointed out that the value of $M_{\beta b}{}^0$ affects the retardation time before this transition. Larger values of $M_{\beta b}{}^0$ will result in longer retardation times. For instance, in the case of $M_{Ab}{}^0 = 0.5$, and $M_{Bb}{}^0 = 0.25$, the first linear regime is prolonged, which corresponds to a longer "frozen" period.

To more clearly understand the dynamics of viscoelastic microphase separation, we now investigate the temporal changes of forces in the average magnitude per lattice: the thermodynamic force $2\phi_A\phi_B\nabla\mu$, the mechanical forces acting on block A, $F_1 = -\phi_B\nabla\sigma^{(A)}$, and as well on block B, $F_2 = \phi_A\nabla\sigma^{(B)}$. We define $F_\phi = |2\phi_A\phi_B\nabla\mu|$, $F_A = |F_1|$, and $F_B = |F_2|$ and show the results of time evolution with various values of $M_{\beta s}{}^0$ and $M_{\beta b}{}^0$ (Figure 5). It can be seen that, for all cases, the three forces have only one maximum, revealing the coupling between the diffusion field and the stress field. The different peak positions indicate the different extents to which relaxation moduli suppress the initial rapid increase in concentration fluctuations.[27] By comparing Figure 5 with Figure 1, the relationship between morphology and the driving force of phase separation can be clearly seen. The regime prior to the force maxima corresponds to the early stage of phase separation, indicating that the systems are in a "frozen" state. The concentration fluctuations accelerate during the intermediate period, and gradually approach a maximum with the attenuation of the driving forces. This observation can be further confirmed by noting that the period in which the forces peak appears to match the transition period between the first and second linear regimes of Figure 4.

Figure 6 shows the time evolution of the scattering function $S(k,t)$ for normal microphase separation of diblock copolymers both including and excluding viscoelasticity for various values of $M_{\beta s}{}^0$ and $M_{\beta b}{}^0$. Excluding viscoelasticity, the time evolution of the scattering function, $S(k,t)$, is in a normal mode for microphase separation for diblock copolymers, as shown in Figure 6a. However, for the viscoelastic system, the increase in the scattering intensity is slowed due to modulus relaxation, so that the scattering intensity is much lower than that in case a, in its early stages. In cases b and d, the patterns of evolution of the scattering functions are quite similar although there are slight differences due to different shear relaxation moduli. The scattering intensity increases at almost the same wavenumber, which corresponds to the inverse of the lamellar thickness, with only one single peak from intermediate stage to the late stage. However, in case c in which there is a bulk modulus difference between the two blocks, in addition to the main peak, a secondary peak appears in the intermediate and late stages of phase separation. The appearance of such a secondary peak is also observed in the viscoelastic phase separation of polymer solutions.[27,29] By comparing it with the morphology evolution in Figure 1c and relating it to previous work in this area,[27,29] it is hypothesized that the main peak corresponds to the characteristic size of droplets of lower bulk modulus B-rich phase. The secondary peak, appearing at a larger wavenumber during the intermediate stage, represents the formation of a thin networklike matrix of the harder phase with a characteristic length smaller than the droplets. Corresponding to the morphology evolution of the B-rich droplets, the higher bulk modulus A-rich phase tends to form a thin networklike continuous matrix, with the peak position of the secondary peak slowly moving in the direction of main peak

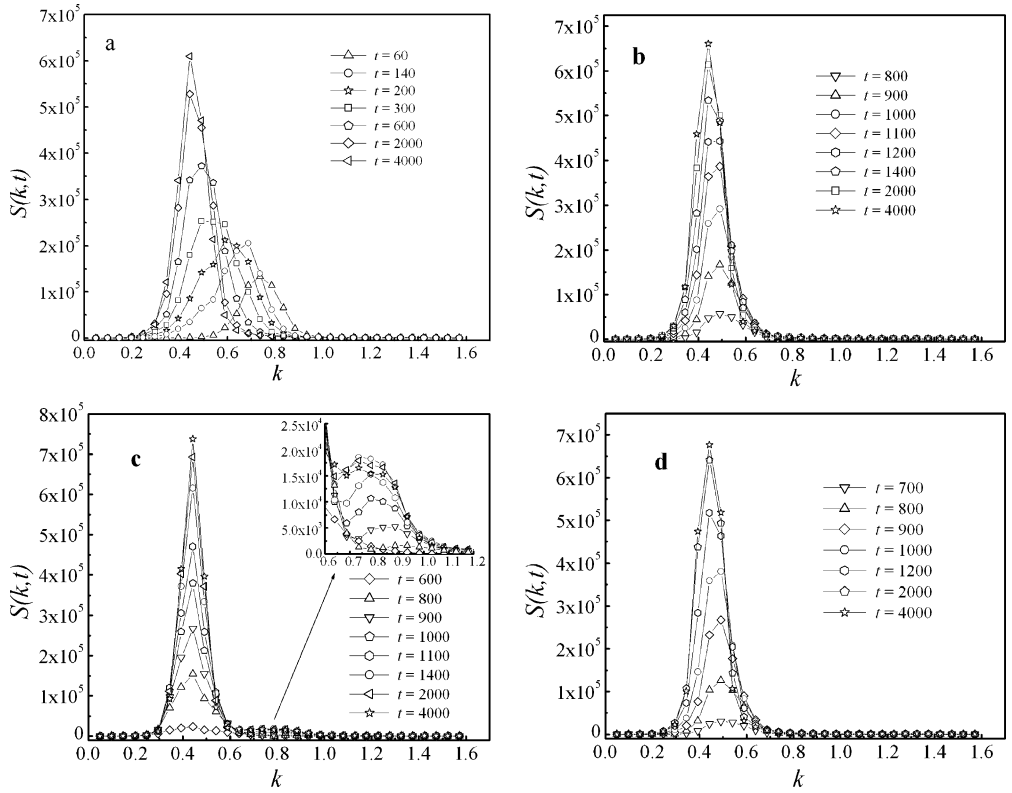

Figure 6. Time evolution of the scattering function for the microphase separation of critical quench ($f = 0.5$): (a) *without viscoelasticity*; (b) $M_{As}^0 = M_{Bs}^0 = 0.5$, $M_{Ab}^0 = M_{Bb}^0 = 0.25$; (c) $M_{As}^0 = M_{Bb}^0 = 0.5$, $M_{Ab}^0 = 0.5$, $M_{Bb}^0 = 0.1$; (d) $M_{As}^0 = 0.5$, $M_{Bs}^0 = 0.1$, $M_{Ab}^0 = M_{Bb}^0 = 0.25$.

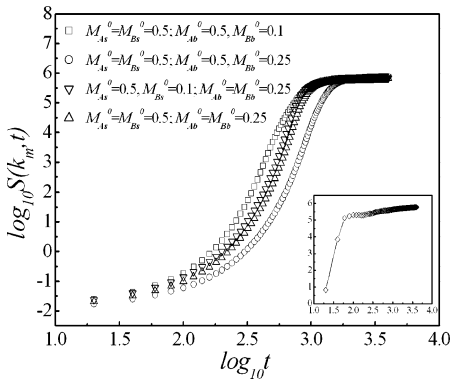

Figure 7. Time evolution of the maximum of scattering function for the microphase separation of critical quench ($f = 0.5$) with various values of $M_{\beta s}^0$ and $M_{\beta b}^0$. The inset shows the evolution without viscoelasticity.

and finally forming a shoulder on the main peak. In the case of $M_{As}^0 = M_{Bs}^0 = 0.5$, $M_{Ab}^0 = 0.5$, $M_{Bb}^0 = 0.25$, where the bulk modulus differences are less (the evolution of the scattering function is not presented here), similar phenomena are observed except that the secondary peak intensity is less than that in case c. It should be noted again that, for all the cases with viscoelasticity, the concentration fluctuation is suppressed in the early stage, so that the scattering intensity is lower than that for the cases in which viscoelastic effects are neglected. To show this suppression more clearly, we show the time evolution of the maximum scattering intensity in Figure 7. In the log−log plot, for the case neglecting viscoelasticity (see inset, Figure 7), the scattering intensity attains a maximum rapidly and immediately. However, for the cases including viscoelastic effects, the growth of the scattering intensity is slow at the beginning, and then gradually approaches its maximum.

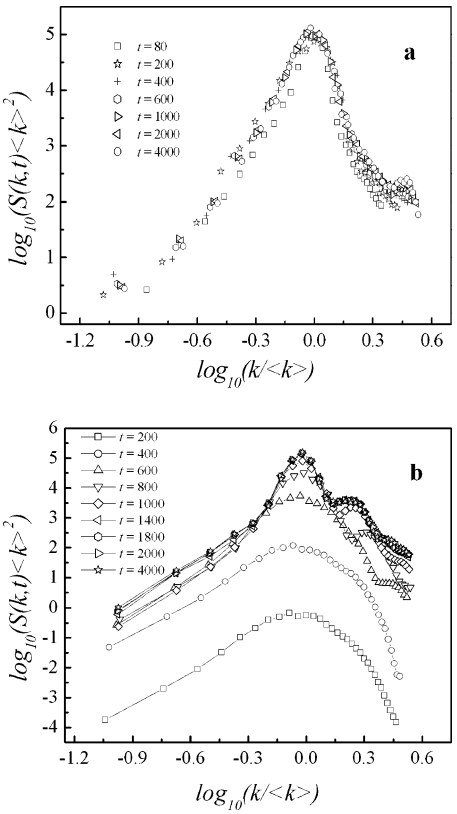

Figure 8. Scaled scattering function: (a) *without viscoelasticity* and (b) $M_{As}^0 = M_{Bs}^0 = 0.5$, $M_{Ab}^0 = 0.5$, and $M_{Bb}^0 = 0.1$ for the case of $f = 0.5$.

Figure 8 shows the self-similarity of the morphologies of microphase separation. For the case neglecting viscoelasticity (Figure 8a), the scaled scattering functions at

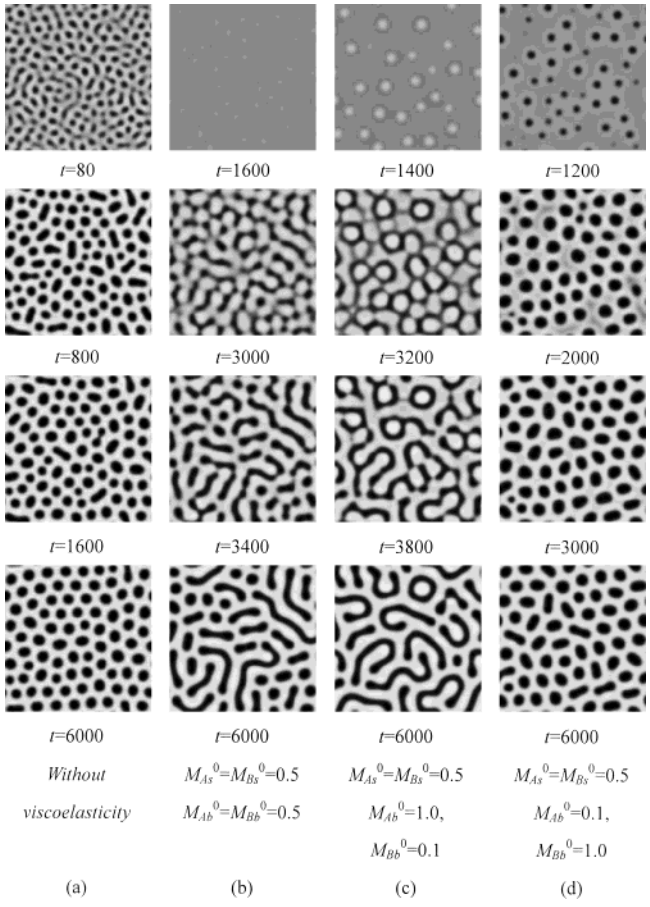

Figure 9. Simulated pattern evolution during microphase separation of off-critical quench ($f = 0.4$) with and without viscoelasticity. A-rich regions are shown by black whereas B-rich regions are shown by white.

different times can be superimposed onto a universal function for the entire process of phase separation, demonstrating the self-similarity of phase separation morphologies. On the other hand, in the cases with differences in the bulk moduli (Figure 8b), this similarity does not exist in the early stages. However, in the intermediate and later stages, the scaled scattering functions can again be superimposed due to the removal of the suppression of viscoelastic effects acting on the concentration fluctuations.

B. Case of $f = 0.4$. For simplicity, here we will now concentrate our attention only on the morphology of the off-critical system. Figure 9 shows the pattern evolution of off-critical compositions for a volume fraction of the A block (ϕ_A) of $f = 0.4$. Different patterns are obtained for various values of $M_{\beta s}^0$ and $M_{\beta b}^0$ (β = A and B). In the case neglecting viscoelastic effects (Figure 9a), A-rich droplets disperse in the B-rich matrix, as is normal for the microphase separation of diblock copolymers. When we take the bulk and shear moduli into consideration, both the dynamics and the morphology are changed. In the early stages, the time evolution of the concentration fluctuation is suppressed to an extent dependent on the relaxation moduli. It should be pointed out that, due to the inherent composition asymmetry of the two blocks ($f = 0.4$), the effects of the modulus differences between them still exists even though both $M_{\beta s}^0$ and $M_{\beta b}^0$ (β = A and B) are identical for the two blocks. Consequently, it is observed (Figure 9b) that in addition to isolated droplets of A-rich phase, some A-rich droplets tend to connect with one another to begin forming a thin lamellar-like morphology. From the symmetric system ($f = 0.5$), we observe that the higher bulk modulus phase tends to form a thin networklike morphology. To confirm that this is the case also for the asymmetric system ($f = 0.4$), we set the bulk modulus of the minor component, A, $M_{Ab}^0 = 1.0$, which is higher than that of the major component, B, $M_{Bb}^0 = 0.1$. It can be seen from the patterns shown in Figure 9c that the component A tends to form a thin lamellar morphology even though the volume fraction of A is only equal to 0.4. From the pattern evolution, it can be seen that the lower bulk modulus B-rich droplets begin to emerge first, and then grow in size, with the A-rich phase being compressed to form a networklike structure. As the microphase separation proceeds further, the B-rich phase eventually forms the continuous phase and the A-rich network is partially broken up. It is obvious that even though the composition is asymmetric ($f = 0.4$), the minor component A has greater tendency to form a lamellar morphology. On the other hand, in the case of the lower bulk modulus A-block, the domains of A-rich phase first emerge from the B-rich matrix and then eventually evolve into isolated A-rich droplets, as shown in Figure 9d. The various patterns of off-critical compositions with $f = 0.4$ further support the hypothesis that the viscoelastic effect is largely responsible for the discrepancy between the mean field calculated and the experimental phase diagrams.

C. Effect of Noise. Thermal noise is necessary for phase separation to occur following a quench into a two-phase region, since a system will not evolve on its own from a truly homogeneous state. Generating that variation by adding a small random fluctuation in volume fraction to each lattice site in the initial state has been shown to reproduce many of the features associated with phase separation in polymer blends.[42,43] The spatial distribution of the domains in late-stage coarsening for the thermal noise case is qualitatively similar to that of the case in which thermal noise is neglected, but increasing the amplitude of the noise leads to a rougher domain topology with a broader and more diffuse interface.[44] Studies of the effects of thermal noise on the phase separation of block copolymer in three dimensions show that thermal noise is essential to generate well-defined spherical phases, but it has no significant effect on the patterns of formation of bicontinuous and lamellar phases.[45] Therefore, it is necessary to investigate the effects of thermal noise on our system. In the present study, a Gaussian random thermal noise term[46] is introduced into the concentration field conservation equation.

The thermal noise has an effect on the concentration fluctuation. Note that increasing the amplitude of the thermal noise weakens the suppression of concentration fluctuations due to viscoelasticity in the early stages of phase separation. The role of thermal noise in morphology development with different M_{Ab}^0 and M_{Bb}^0 is more complicated. When the amplitude of noise is $\epsilon = 0.01$, the morphologies of both the critical and off-critical compositions with noise added are similar to those obtained without it. For both cases shown in Figure 10, parts a and d, the morphologies developed with noise are still similar to those of the cases without noise even though the noise level is as high as $\epsilon = 0.1$. For the cases of Figure 10, parts b and c, the noise has an effect on the morphologies, but the dominant structures are essentially unchanged. For instance, for the critical case

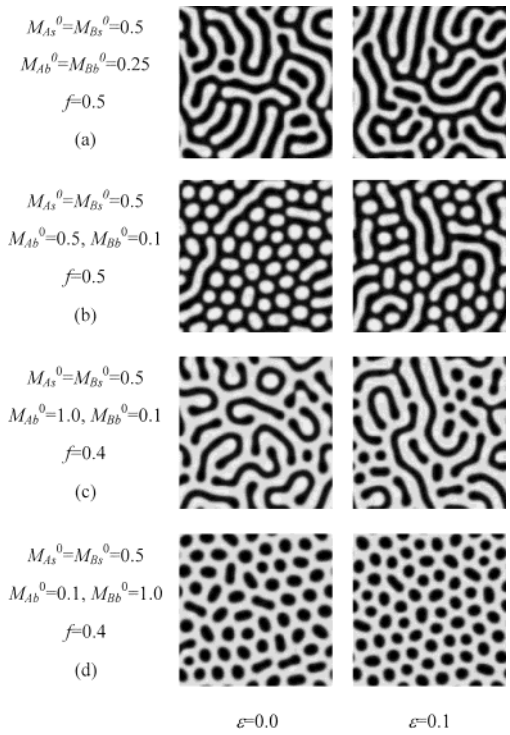

Figure 10. Effects of thermal noise on the morphologies of viscoelastic microphase separation of block copolymer. The time step is 6000. A-rich regions are shown by black whereas B-rich regions are shown by white.

shown in Figure 10b with $\epsilon = 0.1$, the morphology still consists of many dispersed droplets of B-rich phase in the A-rich matrix, even at $f = 0.5$, which is quite different from the normally observed randomly oriented lamellar morphology. Although the asymmetry about $f = 0.5$ for the experimental phase diagram of block copolymers is partly accounted for by the asymmetry in the A and B statistical segment lengths,[47] nevertheless, the viscoelastic effect is thought to be the significant factor responsible for much of the discrepancy between the experimentally measured and mean field theoretically calculated phase diagrams.

IV. Conclusions

In this work, we have investigated the kinetics and morphology of viscoelastic microphase separation of diblock copolymers by extending the viscoelastic model of binary polymer mixtures to diblock copolymers. It is found, in the critical composition case, i.e., $f = 0.5$ and an identical bulk modulus for each block, that the preferred morphology is a randomly oriented lamellar structure. This is the same as in the case in which the viscoelastic effects are neglected, even though microphase separation is strongly suppressed by the stresses in the early stages of phase separation. When there are bulk modulus differences between the two blocks, instead of forming the normal lamellar phase, the higher bulk modulus A-rich phase forms a thin networklike continuous phase, and the lower bulk modulus B-rich droplets disperse in the A-rich matrix even at $f = 0.5$. The time evolution of the area fraction of A-rich phase demonstrates, in the absence of bulk modulus differences, that the area fraction remains constant during the microphase separation process, whereas in the presence of such bulk modulus differences, the area fraction reaches a maximum and then falls to a steady state value that is slightly different from f. Since the abnormal metastable morphology approaches equilibrium very slowly, we can conclude that viscoelastic effects are likely responsible for the deviation of the experimentally measured phase diagram from that predicted by the mean-field theory. In addition, in the presence of bulk modulus differences, the scattering function displays double-peak character during the intermediate stages of phase separation.

In the case of an off-critical system ($f = 0.4$), because of the inherent composition asymmetry, the morphologies are different from cases neglecting viscoelasticity effects, even though both $M_{\beta s}^0$ and $M_{\beta b}^0$ are identical for the two blocks. However, when bulk modulus differences exist, the morphology becomes very different from that of the normal case. This further confirms that the viscoelastic effect may be responsible for the deviation between the experimentally measured and the mean-field theoretically predicted phase diagrams. In addition, over the range of simulation conditions of our study, added thermal noise does not significantly change the dominant phase separation pattern structures for both critical and off-critical compositions.

Acknowledgment. Financial support from the National Natural Science Fund of China, the Special Funds for Major State Basic Research Projects in Ministry of Science and Technology of China, and the China National Special Fund for Excellence in Ph.D. Dissertations are gratefully acknowledged. Y.H., would like to thank Dr. Thomas H. Kalantar for reading through this paper and giving many useful suggestions.

References and Notes

(1) De Gennes, P. G. *Macromolecules* **1976**, *9*, 594.
(2) De Gennes, P. G. *Macromolecules* **1976**, *9*, 587.
(3) Brochard, F.; De Gennes, P. G. *Macromolecules* **1977**, *10*, 1157.
(4) De Gennes, P. G. *J. Chem. Phys.* **1980**, *72*, 4756.
(5) Binder, K.; Frisch, H. L.; Jackle, J. *J. Chem. Phys.* **1986**, *85*, 1505.
(6) Pincus, P. *J. Chem. Phys.* **1981**, *75*, 1996.
(7) Binder, K. *J. Chem. Phys.* **1983**, *79*, 6387.
(8) Onuki, A. *J. Chem. Phys.* **1986**, *85*, 1122.
(9) Doi, M.; Onuki, A. *J. Phys. II (Fr.)* **1992**, *2*, 1631.
(10) Onuki, A. *J. Non-Cryst. Solids* **1994**, *172*, 1151.
(11) Onuki, A.; Taniguchi, T. *J. Chem. Phys.* **1997**, *106*, 5761.
(12) Kumaran, V.; Fredrickson, G. H. *J. Chem. Phys.* **1996**, *105*, 8304.
(13) Tanaka, H.; Nishi, T. *Jpn. J. Appl. Phys. Part 2-Lett.* **1988**, *27*, L1787.
(14) Tanaka, H. *Macromolecules* **1992**, *25*, 6377.
(15) Tanaka, H. *Phys. Rev. Lett.* **1993**, *71*, 3158.
(16) Tanaka, H. *Phys. Rev. Lett.* **1996**, *76*, 787.
(17) Tanaka, H. *Phys. Rev. E* **1997**, *56*, 4451.
(18) Tanaka, H. *Phys. Rev. E* **1999**, *59*, 6842.
(19) Sappelt, D.; Jackle, J. *Physica A* **1997**, *240*, 453.
(20) Sappelt, D.; Jackle, J. *Europhys. Lett.* **1997**, *37*, 13.
(21) Sappelt, D.; Jackle, J. *Polymer* **1998**, *39*, 5253.
(22) Ahluwalia, R. *Phys. Rev. E* **1999**, *59*, 263.
(23) Vladimirova, N.; Malagoli, A.; Mauri, R. *Phys. Rev. E* **1998**, *58*, 7691.
(24) Clarke, N.; McLeish, T. C. B.; Pavawongsak, S.; Higgins, J. S. *Macromolecules* **1997**, *30*, 4459.
(25) Cao, Y.; Zhang, H.; Xiong, Z.; Yang, Y. *Macromol. Theor. Simul.* **2001**, *10*, 314.
(26) Taniguchi, T.; Onuki, A. *Phys. Rev. Lett.* **1996**, *77*, 4910.
(27) Tanaka, H.; Araki, T. *Phys. Rev. Lett.* **1997**, *78*, 4966.
(28) Araki, T.; Tanaka, H. *Macromolecules* **2001**, *34*, 1953.
(29) Zhang, J.; Zhang, Z.; Zhang, H.; Yang, Y. *Phys. Rev. E* **2001**, *64*, art. no. 051510.
(30) Hashimoto, T.; Yamasaki, K.; Koizumi, S.; Hasegawa, H. *Macromolecules* **1993**, *26*, 2895.
(31) Yamaguchi, D.; Bodycomb, J.; Koizumi, S.; Hashimoto, T. *Macromolecules* **1999**, *32*, 5884.

(32) Sakurai, S.; Umeda, H.; Yoshida, A.; Nomura, S. *Macromolecules* **1997**, *30*, 7614.
(33) Ohta, T.; Ito, A. *Phys. Rev. E* **1995**, *52*, 5250.
(34) Ito, A. *Phys. Rev. E* **1999**, *58*, 6158.
(35) Bodycomb, J.; Yamaguchi, D.; Hashimoto, T. *Macromolecules* **2000**, *33*, 5187.
(36) Kim, S. H.; Jo, W. H.; Kim, J. *Macromolecules* **1996**, *29*, 6933.
(37) Matsen, M. W. *J. Phys.: Condens. Matter* **2002**, *14*, R21.
(38) Luo, K.; Yang, Y. *J. Chem. Phys.* **2001**, *115*, 2818.
(39) Liu, F.; Goldenfeld, N. *Phys. Rev. E* **1989**, *39*, 4805.
(40) Oono, Y.; Puri, S. *Phys. Rev. A* **1988**, *38*, 434.
(41) Zhang, Z.; Zhang, H.; Yang, Y. *J. Chem. Phys.* **2001**, *115*, 7783.
(42) Clarke, N. *Phys. Rev. Lett.* **2002**, *89*, 215506.
(43) Glotzer, S. C. *Annu. Rev. Comput. Phys.* **1995**, *2*, 1.
(44) Rogers, T. M.; Elder, K. R.; Desai, R. C. *Phys Rev. B* **1988**, *37*, 9638.
(45) Ren, S. R.; Hamley, I. W. *Macromolecules* **2001**, *34*, 116.
(46) Ball, R. C.; Essery, R. L. H. *J. Phys.: Condens. Matter* **1990**, *2*, 10303.
(47) Matsen, M. W.; Bates, F. S. *J. Polym. Sci., Part B* **1997**, *35*, 945.

MA021504F